Materials Research Proceedings 41 (2024) 802-811 https://doi.org/10.21741/9781644903131-88

Using computer vision to analyse fracture strains of oxide scale layers on a macro level

WESTER Hendrik[1,a *], HUNZE-TRETOW Jan Niklas[1,b], BRUNOTTE Kai[1,c] and BEHRENS Bernd-Arno[1,d]

[1]Institute for Forming Technology and Forming Machines, An der Universität 2, 30823 Garbsen, Germany

[a]wester@ifum.uni-hannover.de, [b]hunze@ifum.uni-hannover.de, [c]brunotte@ifum.uni-hannover.de, [d]behrens@ifum.uni-hannover.de

Keywords: Computer Vision, Fracture Types, Oxide Scale, Tensile Test

Abstract. Hot forging has established itself as an efficient process for the manufacture of highly stressed components. The high semi-finished product temperatures significantly increase the deformation capacity and enable the production of complex geometries. However, high semi-finished product temperatures of up to 1250 °C also lead to increased oxide scale formation. Therefore, oxide scale plays an important role in the context of hot forming processes. Due to the contrasting properties between steel substrates and oxide scale, the appearance of oxide scale affects numerous influencing factors, such as changed friction conditions or thermophysical properties. With increasing interest in numerical process prediction arises the demand to take into account the behaviour of oxide scale in finite-element simulations. In addition to the numerical mapping of the crack behaviour, the challenge in mapping the oxide scale is to determine suitable parameters for describing the failure behaviour. Therefore, this work focuses on a novel procedure to characterise the failure of oxide scale under process relevant conditions of hot forging.

Introduction

Hot forging is widely used to manufacture industrial components. The pre-heating of semi-finished products to temperatures between 800 °C and 1250 °C, significantly decrease the required forming forces and increase formability. However, the high temperatures lead to the formation of oxide scale [1]. Depending on the steel matrix properties like carbon content as well as temperature and oxidation time, different iron oxides like wustite, haematite and magnetite occur. The influence of alloying elements on the oxidation behaviour of steel has been described in [2]. The oxide scale has to be removed which lead to material losses. In addition, the oxide scale particularly influences friction as well as material flow and can lead to an increase of die wear [3]. Furthermore, it was stated that an oxide scale layer can have a protective character. However, protection only takes place if the oxide scale layer is free from defects like cracks or spallation zones [4]. Within hot forming applications, oxide scale is temporarily categorised into primary, secondary and tertiary oxide scale. These different types are formed under different process conditions and react differently to external stresses during the process. They also differ in terms of their volumetric formation. The primary oxide scale is formed during reheating of the material, which usually takes place in conventional furnaces. In case of a slow heating of the material within a furnace before the forming process this type of oxide scale can form unhindered. Therefore, primary oxide scale is also the most pronounced in terms of mass. The primary oxide scale is ideally removed by a high-pressure scale washer or by pre-dipping the samples from the surface, which results in a high material loss. As oxide scale grows immediately in atmosphere, a new thin oxide scale layer develops on the descaled steel surface [5]. Thus, during hot forging in particular the secondary oxide scale has to be considered, which is formed during the transfer into the forming press or between forming steps. Due to shorter oxidation times the layer thickness is small compared to

primary oxide scale. In contrast to thick layers of scale that break up and crack, thin scale deforms evenly with the steel matrix during hot rolling [5]. Based on process conditions like oxidation time and temperature layer thicknesses between 10 µm and 140 µm are formed. Higher oxidation temperatures as well as longer oxidation times leads to an increased oxide scale formation [6]. The development of the oxide scale layer thickness as a function of temperature and oxidation time as well as the alloying elements carbon and chromium was investigated in detail by [6]. Based on the experimental results, a calculation approach was developed to predict the oxide scale layer thickness.

It is known that oxide scale exhibits different deformation behaviour depending on its composition and the existing process conditions. Experimental investigations at elevated temperatures within a range between 900 °C and 1200 °C have shown the different material-specific deformation behaviour. The highest bearable strain was observed for wustite whereas its yield stress has been found to be lower as compared to haematite and magnetite. Haematite has been observed to possess the highest yield stress. Moreover, it has also been found to be the hardest oxide scale component at room temperature with a Vickers hardness of 1000 HV10 as compared to magnetite (600 HV10) and wustite (400 HV10). Furthermore, investigations have shown a significant influence of the strain rate on the forming behaviour [7, 8]. The deformation behaviour of oxidised low carbon steel samples was described in [9]. It was shown, that each phase of the oxide scale changes its deformation behaviour from elastic brittle to plastic at a specific temperature. A strong dependence of the deformation behaviour on the test temperature was also observed during plane strain compression tests of oxidised steel samples under hot rolling conditions. With decreasing test temperature the achievable deformation of oxide scale is reduced [10].

As the oxide scale is hard and brittle compared to the steel substrate it often cracks and separates during forming operations. In [11] diagrams are presented that can be used to predicted different types of oxide scale failure, which can occur under tensile or compressive conditions. It was shown, that depending on the stress conditions that acted on oxide scale, phenomena like delamination, crack formation or spallation could be predicted. The presented diagrams and mathematical approaches are a proper tool to predict the type of failure and can be used as basis for numerical finite element simulations to model oxide scale failure. For realistic modelling, however, specific material data is required, for which suitable test methods are needed that can reproduce process-relevant conditions. In this context, the fracture properties of oxide scale under hot rolling conditions were studied. The experimental tests showed, that oxide scale failure mode is strongly dependent on the temperature and the composition of the oxide scale [12]. The oxide scale fracture was investigated by tensile tests using round tensile specimens. The tests were performed under variation of forming speed and forming temperature. Prior to forming, the samples were subjected to defined oxidation in an air atmosphere. The obtained results indicate two failure modes leading to oxide spallation which are strongly influenced by the temperature, strain rate and strain. The first mode occurs at low temperatures between 850 °C – 900 °C and is characterised by an initial through cracking. This initial cracking is followed by initiation and propagation of a crack along the oxide-metal interface between adjacent cracks. A second failure mode was observed at higher temperature between 900 °C – 1200 °C. As a slipping of the oxide scale relative to the metal surface and ductile behaviour of it has been observed for this mode, it indicated a weak interface and strong oxide scale.

The test methodology presented in [12] provided fundamental findings on the damage of oxide scale layers under conditions relevant to hot rolling. However, the methodology also poses some challenges. For example, it is not possible to clearly determine the time of crack initiation. But, knowledge of the crack initiation time is of particular interest for determining material parameters to describe the damage behaviour such as critical strains. This paper therefore presents a new test

and evaluation methodology to investigate the damage behaviour of oxide scale layers in detail under process-relevant conditions for forging. The data obtained should enable a numerical representation of the damage behaviour of scale in future work.

Materials and Methods

Experimental test procedure. Based on the procedure presented in [12], a tensile test is used to analyse the oxide scale damage behaviour. As described, the focus is on a methodology for determining the time of crack initiation. In addition, it should also be possible to precisely analyse the type of damage. For this purpose, the tensile test is used together with an optical 2D measuring system GOM ARAMIS. By using an optical measuring system, the test can be analysed with both temporal and local resolution. Flat tensile specimens are used in order to be able to analyse as large an area of the specimen as possible. In contrast to the round tensile specimens used in [12], the entire upper side of the specimen can be analysed with flat tensile specimens. The test setup is shown schematically in Fig. 1 (a). A DIL805 A/D+T quenching and forming dilatometer is used in tensile mode for the tensile tests. The tensile specimen is fixed in the left and right specimen holders and then inductively heated using a flat coil. The temperature is controlled via welded-on type S thermocouples. The sample geometry used for tensile tests within forming dilatometer is shown in Fig. 1 (b).

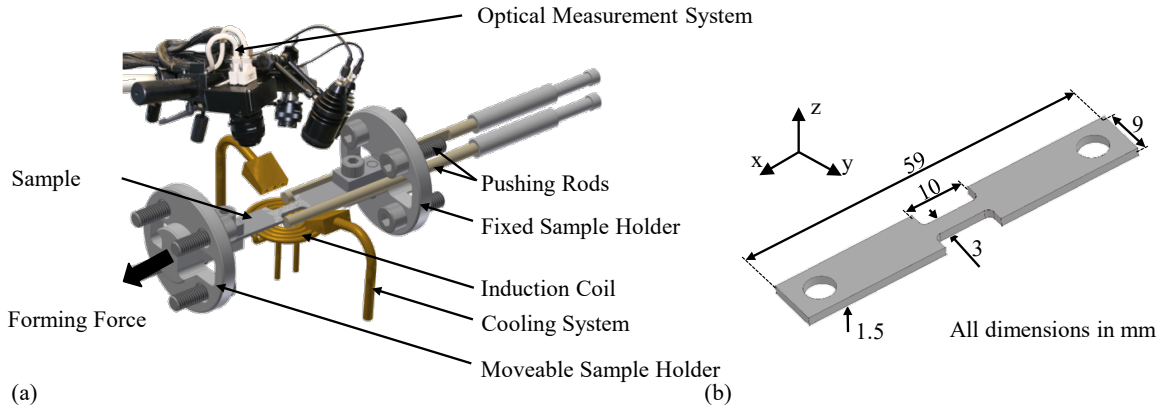

Figure 1 Schematic test setup (a) and sample geometry (b)

The measuring range of the specimen is 10 mm long and 3 mm wide. The thickness of the samples was 1.5 mm. C45 steel was chosen as the material as knowledge on oxide scale growth is already available for this material from previous work. Furthermore, it only consists of the alloying element carbon, so that the influence of carbon on oxide scale damage can be considered later by looking at other alloys such as C15 or C60. During the whole test procedure which includes heating, oxidisation and mechanical testing the sample is fixed between the sample holders within the test chamber. Before the mechanical test under tensile load, the specimens are oxidised in a targeted manner. For this purpose, the samples are first inductively heated with a heating rate of 10 K/s to a specified oxidation temperature under vacuum in the test chamber. After reaching the test temperature, an air atmosphere is set in the test chamber and the specimen is specifically oxidised for a defined time. Once the selected oxidation time has been reached, the test chamber is flooded with nitrogen to prevent further oxidation. For all tests an oxidation time of 120 s were used. After oxidation, the sample is mechanical deformed at a defined test temperature up to a degree of deformation of 0.2. First, the test temperature is chosen to be the same as the oxidation temperature. In further tests, the sample is cooled below the test temperature before the mechanical test. Cooling was carried out at a cooling rate of 5 K/s from oxidation temperature to test temperature using nitrogen. Temperatures were controlled using a thermocouple Type S welded onto the sample surface. A schematic test scheme is shown in Fig. 2. Each test is recorded with the optical measuring system so that time-resolved image series are subsequently available for

analysing the oxide scale damage behaviour. The exposure time setting is of particular importance for the optical analysis of the damage behaviour. This determines the brightness of the respective image. Depending on the test temperature, different settings are required for the exposure time. The maximum possible exposure frequency also goes hand in hand with the exposure time. In principle, exposure frequency should be set as high as possible in order to generate the maximum information content. An exposure time of 1 ms is selected at 1100 °C. This allows the camera's maximum exposure frequency of 160 Hz to be used. At the lowest tested temperature, the exposure time needs to increased up to 13 ms, which leads to an exposure frequency of 65 Hz.

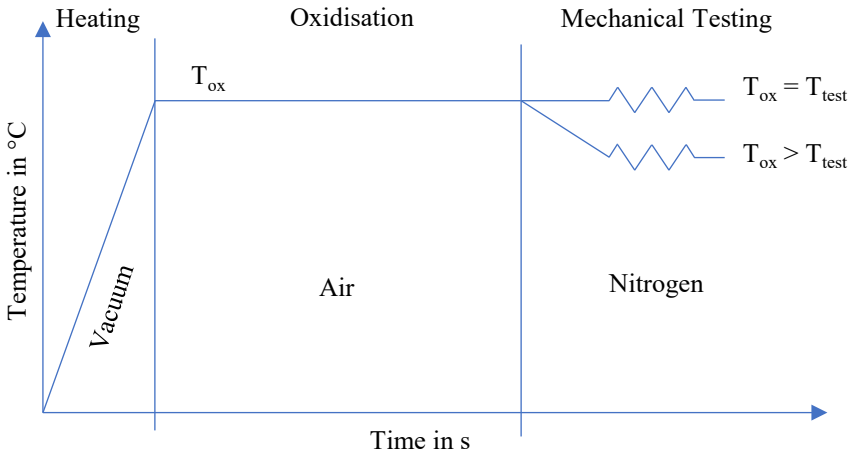

Figure 2 Schematic Test setup

Within this study the influence of different oxidation and test temperatures as well as strain rates were investigated. An overview over the varied parameters, which should represent the hot forging-relevant process conditions, is given in Table 1. A lower test temperature than the oxidation temperature is intended to represent a possible cooling of the oxide scale in air or through contact with the cold tools. Due to the large combination of parameters, the test matrix was not initially subjected to a full factorial test. When selecting the parameters, the focus was on the individual consideration of various effects such as the influence of the oxidation temperature, the influence of cooling after oxidation or the influence of the strain rate. The tested parameter combinations are discussed in the results section. Each test was repeated 5 times for statistical validation

Table 1. Test Matrix

Oxidation temperature [°C]	1100, 1050, 1000, 950, 900, 850
Test temperature [°C]	1100, 1050, 1000, 950, 900, 750, 600, 450
Strain rate [s^{-1}]	0.01, 0.05, 0.1
Oxidation time [s]	120

Evaluation Method: Following the test, the Aramis system delivers an image sequence. Each image is saved in a separate file in greyscale pixel format with a size of 2400 pixel in x direction and 1728 pixel in y direction. This means that there is a two-dimensional arrangement of values, which can be integers between zero (black) and 255 (white). As large amounts of data are generated in the course of the test evaluation, a semi-automated Python script was developed using SciPy library for data processing based on computer vision approaches.

First, the crack initiation point is determined automatically. The images are called up one after the other in chronological order and analysed for their characteristics. To speed up this iteration, not the consecutive images are called up, but every 40th image in a first loop. If a crack is found,

a more precise search is carried out in two stages between the chosen image and the previously analysed image. For crack identification, a search area is first defined, the so-called crack identification box (CIB). This is done for the initial image of the image series. In this image, a rectangular area is defined which covers the gauge area of the sample. However, the CIB should be smaller than the gauge area of the sample in order not to detect localised changes at the sample edges. To determine the CIB, a horizontal Sobel filter is applied to the image array to emphasize horizontal edges. This creates a gradient image from the original image. The areas of highest intensity are where the brightness of the original image changes the most and therefore represent the sharpest edges [13]. Depending on the orientation, the edges take on a very small or very large value in the array of the image. The Python script utilises this property and extracts the gauge area using defined limit values. Fig. 3 (a) shows the processed image and the defined CIB. The generated CIB can also be recognised as a superimposed rectangle and the vertical line, which is used to identify the horizontal sample limits. An initial analysis of the tests showed that, for test temperatures between 849 °C and 1051 °C ductile cracks can be observed. Outside this temperature range brittle cracks occur. Furthermore, a test temperature below 849 °C thermal shifts due to cooling and at temperatures above 1051 °C formation of bubbles can be observed. To consider the different failure behaviour and the described phenomena two methods were used for crack identification. For temperatures within the defined range, where ductile cracks can be observed, a mean value kernel with a size of (20,1) and a stride or step size of the kernel of (1,5) is used. Here, the size of the kernel describes the size of the mask to which the filter is applied and the stride the shift of this mask. The lines of the convolved image are then considered and a Savitzky–Golay filter is applied to the individual lines to reduce noise [14, 15]. Subsequently the gradient is calculated. A crack is characterised by the fact that a local maximum follows a local minimum in a small interval, or vice versa. Because cracks are known to propagate in a vertical direction, the mean value filter with its vertical shape can be used to reduce the noise. Due to its shape, a crack will exhibit a characteristic value in the filtered matrix despite the filter (Fig. 3 (b)).

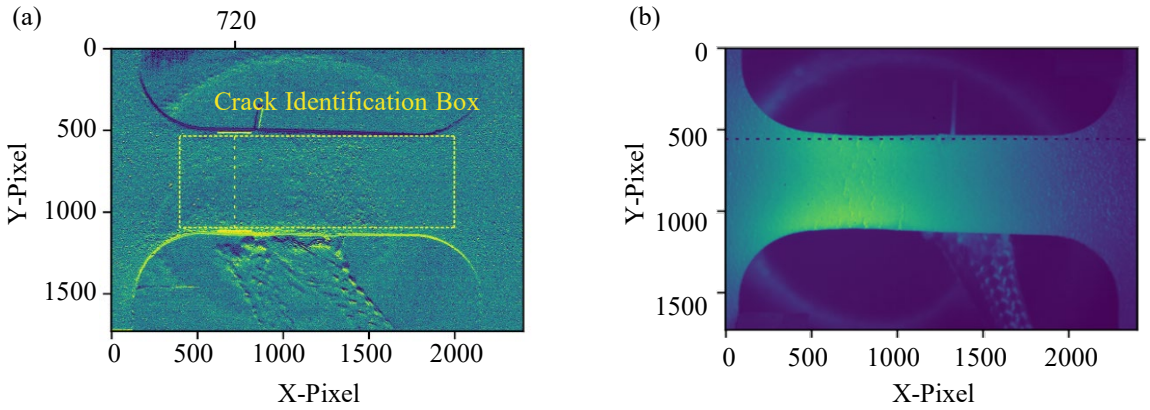

Figure 3 Definition of Crack Identification Box based on the first image (a) and processed image for identification of ductile cracks within the oxide scale (b)

If the test temperature is outside an interval of 849 °C and 1051 °C, a different crack detection is performed. This is necessary because phenomena like bubbles and thermal shifts can lead to the detection of vertical edges on the sample, which can be incorrectly interpreted as cracks. However, as this is a static occurrence, the same information content is present on image *i* and on a previous image. Therefore, in addition to the current image (*i*), the penultimate image (*i-2*) is also used. The two images are first filtered for vertical edges using a Sobel filter. This is shown in Fig. 4 (a) for image *i*. The two filtered images are then subtracted from each other to determine a total gradient of the vertical edges. The static effects are filtered out by subtraction like shown in Fig. 4 (b). As

the cracks in this temperature range are "brittle" cracks that propagate rapidly, they can be identified using this method with a step size of 2. Using this processed image based in image *i* and image *i-2* the same operations are used for crack identification as for ductile cracks. However, the kernel has the size (160,1) and takes place in a stride of (1,5). As brittle cracks are more pronounced, they can be better detected using the method described. A larger kernel can therefore be used. As with "ductile" cracks, the shape of the crack is used for identification. Cracks are searched for along the horizontal. To reduce the noise, the Savitzky–Golay filter is applied again. The final identification of a crack is carried out analogously to the ductile cracks by the sequence of minima and maxima. To avoid errors, the identified cracks are checked and, if necessary, adjusted by the user as part of the evaluation process.

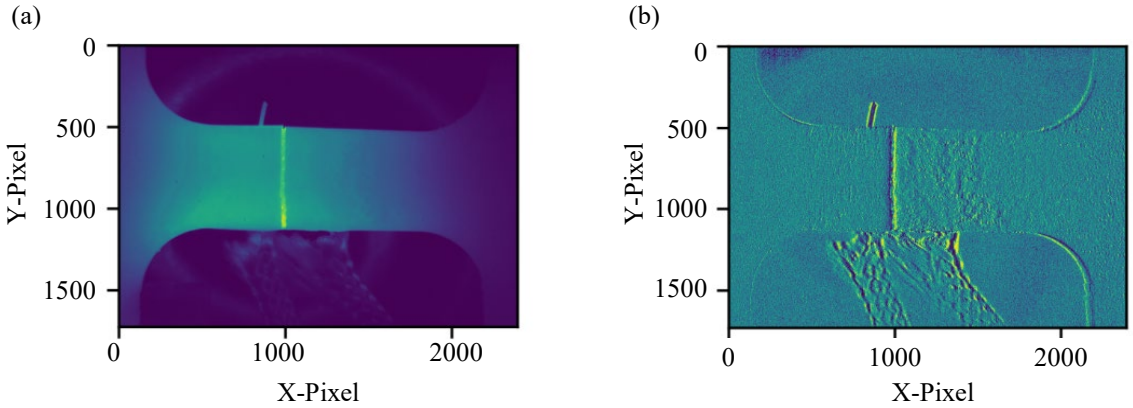

Figure 4 Processed images to identify brittle cracks based on image i (a) and total gradient image using image i and i-2 (b)

Finally, the sample is measured optically. The first image, i.e. the image in which there is no deformation, and the image that represents the time of crack initiation are used. The measurement is based on the distance between the shoulders of the sample. For this purpose, a Sobel filter is applied to both images to emphasise vertical edges. An average kernel of size (40,1) is subsequently applied to both filtered images along a line to take into account the shape of the shoulder as a vertical line and reduce noise. The edges of the shoulder can be identified via the maximum or minimum of the array starting from the beginning or end. Fig. 5 shows an example of this for the "brittle" crack. The edges of the sample shoulders are clearly recognisable in all images and were correctly identified by the algorithm. Finally, the strain is calculated using the measured sample lengths. The sample length itself is taken as a unitless proportion of the total image width. A critical strain which leads to failure of the oxide scale layer is calculated as the change in length (l_1-l_0) of its original length (l_0). As incorrect crack detection cannot be completely prevented, a final check is carried out by manual user control of the identified crack time and the determined line for measuring the change in length. For this purpose, the corresponding images are displayed after the evaluation. This was carried out for all evaluated tests, with the algorithm demonstrating a very high identification rate.

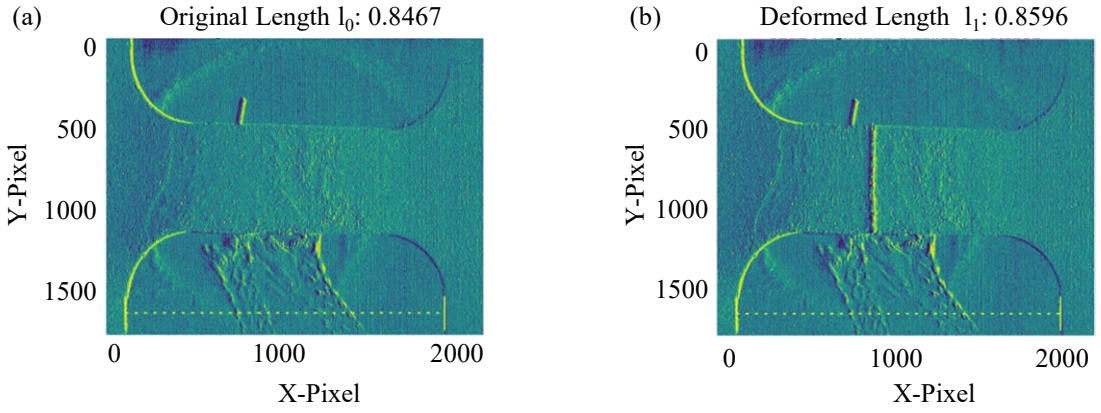

Figure 5 Optical measurement of length change for fracture initiation

Results

The tensile tests performed on defined oxidised samples were analysed using the evaluation tool. Samples showing an initial failure of the oxide layer were removed from the evaluation. The focus was on analysing the fracture behaviour and determining the characteristic critical strain at crack initiation. The Figure 6 shows the critical strain for different oxidation temperatures or test temperatures. In this case, the oxidation temperature was chosen to be the same as the test temperature. The strain rate was 0.01 s^{-1}.

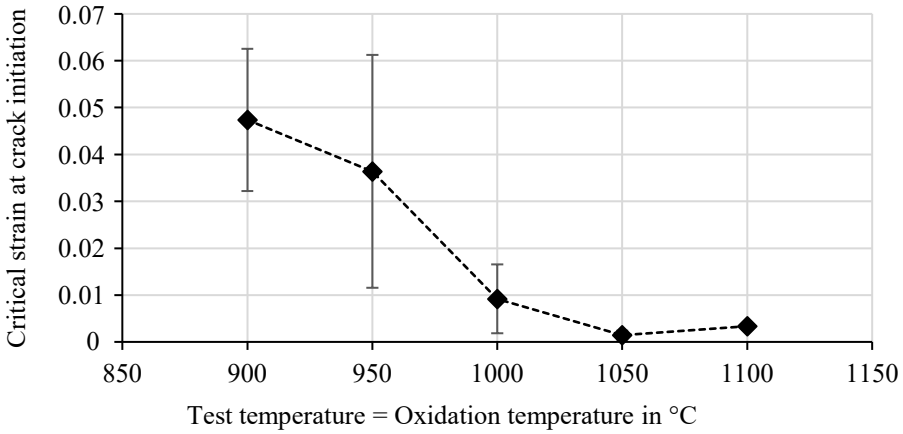

Figure 6 Influence of temperature on critical strain at crack initiation for a strain rate of 0.01 s^{-1}

The curve shows a decrease in the achievable critical strain of the oxide scale layer with increasing temperature. Low temperatures in the range of 900 °C - 950 °C indicate a ductile behaviour of the oxide scale layer. In contrast, high temperatures of above 1000 °C indicate brittle fracture behaviour. This behaviour can also be seen in the fracture images of the oxide scale layer. Fig. 7 shows a sample at the time of crack initiation (a) and at a later point in time (b) for a test temperature of 900 °C and a strain rate of 0.01 s^{-1}. It is clearly visible that several fine cracks form on the sample, but these do not increase significantly even with ongoing deformation. Brittle cracking or spallation of the oxide scale layer is also not observed. In addition, Fig. 7 shows a sample for a test temperature of 1100 °C for a strain rate of 0.01 s^{-1} at the time of crack initiation (c) and at a later time (d). At the time of crack initiation, a single brittle crack can be seen running down the center of the entire sample. As the deformation progresses, a clear widening of the crack can be seen. Once a crack has formed, the oxide scale layer does not appear to undergo any further plastic deformation. This leads to an enlargement of the crack. Furthermore, this indicates a sliding of the oxide scale layer on the steel base substrate, which continues to deform plastically.

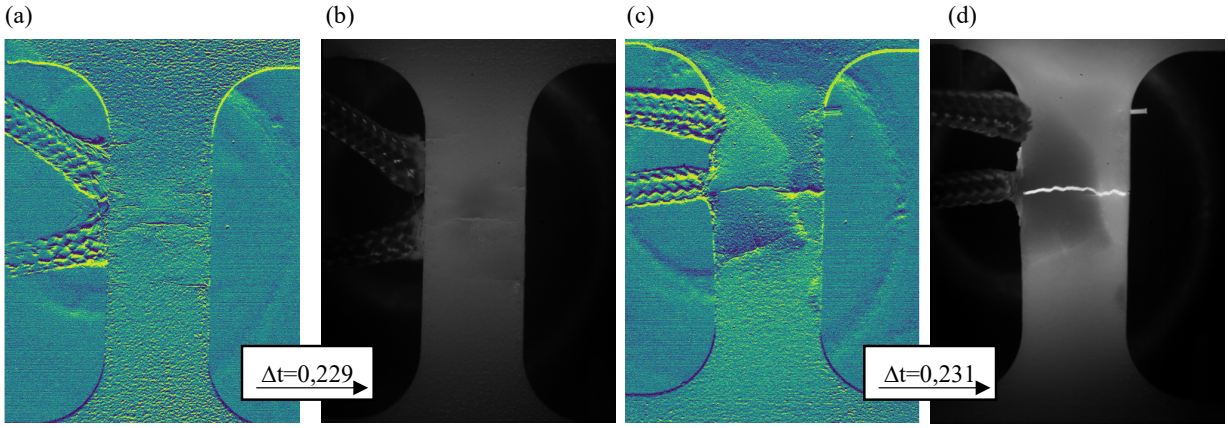

Figure 7 Ductile oxide scale failure at a test temperature of 900 °C at crack initiation (a) and at a later stage (b) as well as at a test temperature of 1100 °C at crack initiation (c) and at a later stage (d) for a astrain rate of 0.01 s^{-1}

Fig. 8 (a) shows the influence of the strain rate on the achievable strain within the oxide scale layer for a constant oxidation temperature of 900 °C. Even in this case, the test temperature was chosen to be the same as the oxidation temperature. It can be seen that for low strain rates in the range 0.01 s^{-1} to 0.05 s^{-1} no significant effect can be observed. However, when the strain rate is increased to 0.1 s^{-1}, there is a considerable decrease in the critical strain, which indicates a change in the fracture shape from ductile to brittle.

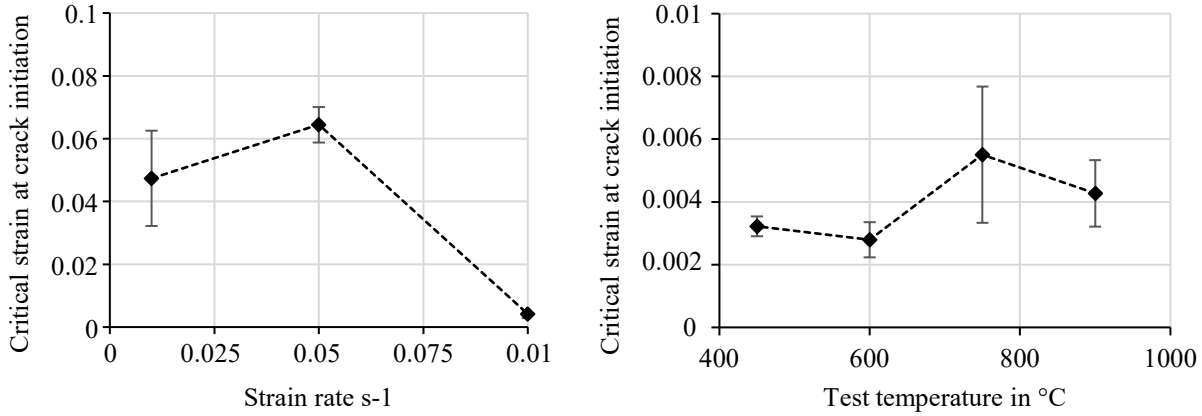

Figure 8 Influence of strain rate on oxide scale failure for a test temperature of 900 °C (a) and influence of test temperature on oxide scale failure for an oxidation temperature of 1050 °C and a strain rate of 0.01 s^{-1} (b)

Finally, the influence of different test temperatures with constant oxidation parameters was investigated. This case illustrates oxidation of a heated semi-finished product, for example during transfer and cooling of the oxide scale by air or contact with the cold tools. Furthermore, in this case the constant oxidation conditions result in an oxide scale layer with the same oxide scale layer thickness and composition. For this purpose, an oxidation temperature of 1050 °C was selected and the samples were cooled to test temperatures between 900 °C and 450 °C in accordance with the procedure described. All tests were carried out at a strain rate of 0.01 s-1. Compared to the other samples, these tests therefore always show a comparable oxide scale layer thickness and composition. The influence of different test temperatures on the achievable critical strain is shown in Fig. 9 (b). In the test temperature range between 600 °C and 950 °C, no significant influence of the temperature on the critical strain can be observed. However, a temperature of 400 °C leads to a significant decrease in the achievable strain. Overall, the critical degrees of deformation are well below the values observed for higher temperatures (Fig. 6). The degrees of deformation achieved

indicate a brittle failure of the oxide scale. This is also illustrated by the images of the sample at 900 °C (a, b) and 480 °C (c, d) shown in Fig. 10.

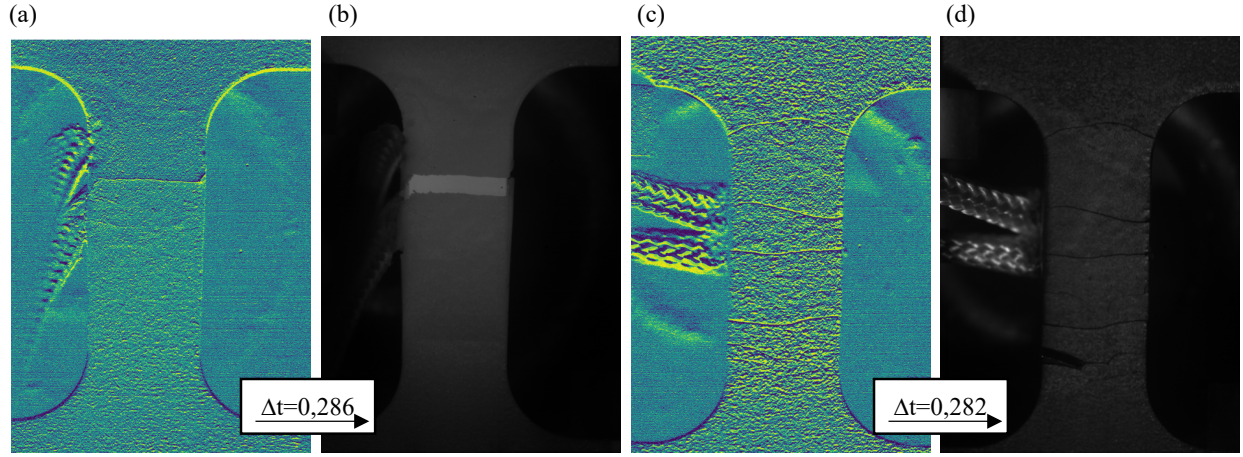

Figure 9 Oxide failure at a test temperature of 900 °C at crack initiation (a) and at a later stage (b) and at a test temperature of 450 °C at crack initiation (c) and at a later stage (d) for an oxidation temperature of 1050 °C and a atrain rate of 0.01 s-1

Both test temperatures show a brittle crack pattern and an enlargement of the crack with increasing mechanical load. At a test temperature of 450 °C, several fine cracks can be seen in the sample, which increase in size continuously. This indicates a lower strength of the oxide scale or a stronger bonding of the oxide scale to the steel substrate. Unlike at 900 °C, it is not possible for a larger oxide scale layer to slide off.

Summary

In this work, the damage behaviour of oxide scale on C45 steel was analysed under hot forging-relevant process conditions. For the local and temporally resolved investigation of the damage, flat tensile tests were carried out on specifically oxidized samples, which were recorded with an optical measuring system. An evaluation algorithm based on computer vision approaches was developed to evaluate the recorded image series. The subsequent analysis of the tests carried out showed that the oxide scale layer exhibits different forms of damage depending on the temperature and strain rate. Low oxidation temperatures result in a rather ductile behaviour of the oxide scale layer, whereas higher oxidation temperatures tend to lead to a brittle damage behaviour. A more ductile behaviour can also be observed at low strain rates. Higher strain rates result in a brittle fracture of the oxide scale layer. However, the work of [6] reveals that even with the same oxidation time, different oxidation temperatures lead to different oxide scale layer thicknesses and compositions. Thus, in further work, the oxide scale layer thickness and composition are therefore to be calculated based on the work of [16] and correlated with the results obtained on damage behaviour. Tests with comparable oxidation parameters and thus comparable oxide scale layer thicknesses and compositions also showed an influence of the test temperature. A decrease of achievable critical strain was observed for reduced test temperatures. In order to make more holistic statements about the effects and to analyse interactions between individual effects in more detail, the test matrix is to be expanded in further work.

Acknowledgement

The authors thank the German Research Foundation (DFG) for the financial support of the project “General modelling of material behaviour and surface modifications for FEM analysis of the die forging of carbon steels” (Project number 316273316).

References

[1] B.-A. Behrens, R. Kawalla, B. Awiszus, A. Bouguecha, M. Ullmann, M. Graf, C. Bonk, A. Chugreev, and H. Wester, Numerical Investigation of the Oxide Scale Deformation Behaviour with Consideration of Carbon Content during Hot Forging,Procedia Engineering 207 (2017) 526–531. https://doi.org/10.1016/j.proeng.2017.10.816

[2] R. Kawalla and F. Steinert, Untersuchung des Einflusses von Prozessparametern in der Fertigstraße auf die Tertiärzunderausbildung,Materialwissenschaft und Werkstofftechnik 1 (38) (2007) 36–42. https://doi.org/10.1002/mawe.200600075

[3] L. Luong and T. Heijkoop, The influence of scale on friction in hot metal working,Wear 71 (1) (1981) 93–102. https://doi.org/10.1016/0043-1648(81)90142-3

[4] M. Schütze, Mechanical properties of oxide scales,Oxid Met 44 (1-2) (1995) 29–61. https://doi.org/10.1007/BF01046722

[5] H. Utsunomiya, S. Doi, K. Hara, T. Sakai, and S. Yanagi, Deformation of oxide scale on steel surface during hot rolling,CIRP Annals 58 (1 (2009) 271–274. https://doi.org/10.1016/j.cirp.2009.03.050

[6] G. Korpała, M. Ullmann, M. Graf, H. Wester, A. Bouguecha, B. Awiszus, B.-A. Behrens, and R. Kawalla, Modelling the influence of carbon content on material behavior during forging. DOI=10.1063/1.5008226.

[7] Graf, M. (2013. *Modellierung des Umformverhaltens von Zunder entlang der Prozesskette Warmband*. Freiberger Forschungshefte. B, Werkstofftechnologie 353. Technische Universität Bergakademie Freiberg, Freiberg.

[8] M. Graf and R. Kawalla, Scale Behaviour and Deformation Properties of Oxide Scale during Hot Rolling of Steel,KEM 504-506 (2012) 199–204. https://doi.org/10.4028/www.scientific.net/KEM.504-506.199

[9] J. Favergeon, G. Moulin, A. Makni, and L. Lahoche, The Effect of Oxide Scale on the Mechanical Behavior of Low Alloyed Steel at High Temperature, MSF 522-523 (2006) 401–408. https://doi.org/10.4028/www.scientific.net/MSF.522-523.401

[10] L. Suárez, Y. Houbaert, X. V. Eynde, and R. Colás, High temperature deformation of oxide scale,Corrosion Science 51 (2) (2009) 309–315. https://doi.org/10.1016/j.corsci.2008.10.027

[11] M. Schütze, P. F. Tortorelli, and I. G. Wright, Development of a Comprehensive Oxide Scale Failure Diagram,Oxid Met 73 (3-4) (2010) 389–418. https://doi.org/10.1007/s11085-009-9185-7

[12] M. Krzyzanowski and J. H. Beynon, The tensile failure of mild steel oxides under hot rolling conditions,Steel Research 70 (1) (1999) 22–27. https://doi.org/10.1002/srin.199905596

[13] W. Gao, X. Zhang, L. Yang, and H. Liu (2010, An improved Sobel edge detection. In 3rd International Conference on Computer Science and Information Technology. IEEE) 67–71 (2010). https://doi.org/10.1109/ICCSIT.2010.5563693

[14] A. Savitzky and M. J. E. Golay, Smoothing and Differentiation of Data by Simplified Least Squares Procedures,Anal. Chem. 36 (8) (1964) 1627–1639. https://doi.org/10.1021/ac60214a047

[15] R. Jardim and F. Morgado-Dias, Savitzky–Golay filtering as image noise reduction with sharp color reset,Microprocessors and Microsystems 74 (2020). https://doi.org/10.1016/j.micpro.2020.103006

[16] T. Bergelt, M. Graf, J. N. Hunze, B.-A. Behrens, and T. Lampke, Investigation of scale properties and layer growth depending on the carbon and chromium content in steel, European Oxide Scale Conference (2022). https://doi.org/10.5281/zenodo.10138002